IEEE Access
Multidisciplinary | Rapid Review | Open Access Journal

Received May 13, 2020, accepted June 25, 2020, date of publication July 1, 2020, date of current version July 14, 2020.

Digital Object Identifier 10.1109/ACCESS.2020.3006444

Electromagnetic Technique for Hydrocarbon and Sand Transport Monitoring: Proof of Concept

YESSICA ARELLANO[1], ANDY HUNT[2], AND LU MA[2]
[1]Fluid and Complex Systems Research Center, Coventry University, Coventry CV1 5FB, U.K.
[2]iPhase Ltd., Intec Business Park, Basingstoke RG24 8NE, U.K.

Corresponding author: Lu Ma (luma@iphaseflow.com)

This work was funded by iPhase Ltd. who also provided material resources in the form of hardware, software and experimental facilities.

ABSTRACT Electromagnetic metering offers significant promise in the measurement of low-conductivity medium like in multiphase flow. Such measurements rely on the measurement of conductivity contrasts formed by two medium of substances, one substance being conductive and the other being non-conductive. In these conditions, it is assumed that the permittivity-induced displacement current is small compared to eddy current induced by conductivity, therefore the displacement current is usually ignored. The present study demonstrates, through solution of the electromagnetic forward problem and pilot tests, that the temporal, spatial and frequency related permittivity and conductivity changes are all captured by the induced electrical voltage measurement. Permittivity reflects in the amplitude and the conductivity reflects both in the amplitude and the phase angle of the voltage. The weight of each parameter to the voltage measurement is studied here. The findings of the study disclose that an electromagnetic metering system may offer advantages in continuously monitoring and measuring hydrocarbon contents and solid concentrations via both the amplitude and phase shift changes.

INDEX TERMS Conductivity, electromagnetic measurements, fluid flow measurement, permittivity.

I. INTRODUCTION

The volatility of oil prices and the finiteness of the resources have challenged the petroleum industry to change its traditional operating schemes in order to optimise their processes and increase the energy efficiency and sustainability of the fields. The development of new technologies has aided oil companies to shift their traditional production strategies and make significant savings in exploration and production activities [1]. Multiphase flow measurement (MFM) plays a key role in providing solutions to the oil and gas industry enabling alternative production approaches for the optimization of their processes. After over two decades since the implementations of the first generations of flow meters, MFM is now present in most transport process within the value chain of the petroleum industry, going from well clean-up operations to production allocation and custody transfer [2].

Available MFM systems are intrinsically complex leading to existing commercial devices with uncertainties ranging from 5% to 20% or more on each of the flowing phases. Most of these MFM developments, target volume fraction and velocity measurements of water and hydrocarbon mixtures. On the opposite spectrum, measurement of slurries containing high soil content has proven challenging for the industry due to the damage caused to traditional inline flow meters [3]. In this regard, this work proposes the use of electromagnetic measurements as a new alternative technology to monitor multiphase flow transport. The present study evaluates the feasibility of an electromagnetic technique for measurement of the electrical properties of the fluids including those containing inorganic suspended particles. The implementation of electrometric metering is motivated by the intrinsic characteristics of the technology in terms of non-invasiveness, low cost, high speed and installation adaptability that answer to the requirements of the industry and address the challenges that commercial MFM solutions face.

The principle of operation of electromagnetic induction systems is based on the energisation of at least one excitation sensor via a sinusoidal alternating signal. This generates an electromagnetic field that interacts with the fluids within the pipe. Eddy currents are formed in the body of the electrically conductive phase, disturbing the initial field distribution and producing a secondary magnetic field. The resultant changes are measured on the periphery of the pipe by one or more detection coils.

The associate editor coordinating the review of this manuscript and approving it for publication was Chao Tan.

Electromagnetic measurements have yielded the development of tomography technologies for the measurement of conductivity contrasts, like for example Magnetic Induction Tomography (MIT) [4]. The first metering system based on electromagnetic induction for water content measurement in two-phase flows dates from 1995 [5]. Correspondingly, further work has mainly focused on measurements of two-phase flows with one conductive substance, i.e. saline water, and one non-conductive phase, like gas or oil. These work include the imaging of conductivity contrast by using static phantom setup [6], semi-static experimental verification [7], and water continuous two phase flow experiments [8]. In the present study, the former two approaches are used to demonstrate the feasibility of broadening the niche of electrometric induced systems for measurement of multiphase flows containing not only water and hydrocarbons but also inorganic particles like sand. The present work assesses the signal response of a dual sensor system to changes in the electromagnetic properties of the medium via a numerical solution of the electromagnetic forward problem. Results from simulations and experiments are used here to identify the response of the measured signal to changes in both the electrical and the dielectric properties of the medium, for measurement of non-conductive phases i.e. oil, gas and sand, which could potentially lead to enhanced three-phase measurement accuracy.

The proposed approach departs from that used in existing electromagnetic meters which measure conductivity contrasts solely. Conductivity measurements are based on the extendedly exploited method in which the displacements currents induced in the medium are neglected for cases where $\sigma \gg \omega\varepsilon$ (σ is the conductivity, ω is the angular frequency, and ε is the permittivity) [9]. Displacement currents account for the effect of the permittivity of the fluids, which in hand with conduction currents, give rise to the secondary induced field described above. Paradoxically, only a few studies have addressed the effect of permittivity in electromagnetic measurements, all of which are limited to the biomedical field [10]–[15]. However, irrespective of the application field, in processes where permittivity and conductivity vary in both the temporal and the spatial domains, like in multiphase flow transport, both the displacement and the eddy currents contribute to the induced magnetic field. Therefore, the effect of the displacement currents should not be ignored.

Previous studies have demonstrated the feasibility of deriving the permittivity from electromagnetic measurements using inclusions of skin depth much larger than the sample dimensions [16]. However, it was reported that when the skin depth of the sample is comparable with the thickness of the inclusions the measured signals departed widely from the theory. This results in the need for a more detailed analysis of the effect of the permittivity on the induced signal. Furthermore, the effect of permittivity on the received measurements is largely influenced by the operating frequency of the measuring system. For low excitation frequencies, some authors have suggested the separation of the contribution of the different electrical parameters based on their dependence on frequency [13], [14]. Conversely, in the limited published literature on permittivity measurement within low conductive contrasts, the components of the signal are de-multiplexed and the effect of the properties are evaluated separately for the imaginary and real components [10], [11], [16].

In the following sections, a thorough evaluation of the electromagnetic signals induced by various fluids and phase fraction distributions is presented. As a result, the weight of the conductivity and permittivity on the induced signals is assessed for the first time and the effect of the frequency on the absolute and the demodulated signals is presented. The identification of the signal response to changes in electromagnetic properties of the fluids would result in an enhanced multiphase measurement technique. Furthermore, the use of a single system to measure conductive and non-conductive phases could potentially remove the need to co-locate separate devices for measurement of non-conductive mediums like explored in [17].

II. CONSIDERATIONS ON PERMITTIVITY, CONDUCTIVITY AND ELECTROMAGNETIC SIGNALS

The electromagnetic problem is governed by the set of Maxwell's equations. The measured electromagnetic signal combines information from the conduction and the displacement currents within the pipe. The background voltage measured by the receiving coil, in absence of an inclusion, lags 90 deg from the driving current for lossless coils. When an inhomogeneity flows through the pipe, the change in conductivity and permittivity is picked up by the receiving coil.

As previously stated, the simplified model, denominated the eddy current problem, has been broadly used in low-conductivity imaging. The eddy current problem is a quasi-static approximation of the full electromagnetic problem. At high excitation frequencies, the phase shift due to changes in the properties of the inclusion for low conductive mediums is very small. Hence, the eddy current approximation has been considered valid for small inclusion dimensions and high conductivities ($\sigma \gg \omega\varepsilon_0\varepsilon_r$). Using the small-angle approximation, the phase change is assumed to be proportional to the real part of the induced voltage and is approximately equal to the imaginary part [16], [18].

However, the quasi-static approximation involves intrinsic inaccuracies as reported in [19], [20]. In order to account for the effect of permittivity on the received signal, an accurate relationship between the dielectric properties and the measurements needs to be solved. This approach involves rejecting the eddy current approximation and retaining the displacement current term in the Ampere circuital laws with Maxwell addition. For current-driven coils, the displacement currents, cause an imaginary component in-phase with the background voltage whereas conduction currents give rise to a real in-quadrature part that lags 90 deg the induction current. Deriving Maxwell's equations by the introduction of the combined magnetic and electric scalar potentials, and

using the temporal gauge yields:

$$\nabla \times \left(\mu^{-1} \nabla \times A\right) + (j\sigma + \omega\varepsilon_0\varepsilon_r)\,\omega A = J_s \qquad (1)$$

where J_s is the current density of the source, and the electrical properties are given by the permeability (μ), the conductivity (σ), and the permittivity ($\varepsilon = \varepsilon_0\varepsilon_r$). A is the magnetic vector potential used to convert the governing equations into second-order differential equations.

In Equation (1) the term $j\sigma + \omega\varepsilon_0\varepsilon_r$ is the complex conductivity which comprises the residual static conductivity and the polarization losses due to dispersion. The relative permittivity is directly related to the macroscopic properties of the materials, like polarization or capacitance. The inclusion of the dielectric properties in (1) reflects the contribution of the fluid properties to their polarization when subjected to an electrical field.

There are a number of sources that originate the material polarization at different frequencies. This frequency dependence of the relative permittivity contributes to that, in any given material, a number of polarization sources will activate at different frequencies [21]. Considering that the electronic and atomic effects do not change significantly, dipolar, space charge, and ionic are the main contributors to polarization mechanism arising at RF frequencies of interest [22].

The following sections address the effect of the macroscopic effective dielectric permittivity distribution of hydrocarbon mixtures in electromagnetic signals. Due to the inherent complexity of the multiphase flow phenomena i.e. the complex interfacial polarization phenomena arising from multiple fluids in contact, in addition to the presence of conductive materials, the present work focuses on the macroscopic electromagnetic behaviour of multiphase mixtures. The concept of macroscopic effective permittivity assumes that a heterogeneous mixture interacts with electromagnetic excitations as if it were a homogeneous medium [23]. This concept is valid, from an electromagnetic perspective, only if the particles inside the mixture are small compared to the wavelength of the excitation field, which is the case of the present work. In correspondence, this study focuses on excitation frequencies below 20 MHz which are typically used for measurement of fluid conductivity in a multiphase flow. Consequently, the wave propagation effect evidenced in electromagnetic induced measurements at higher excitation frequencies can be neglected within the scope of the present study [24].

The following sections detail the effect of frequency on the induced currents when multiphase mixtures of different permittivities and conductivities are flowing through the pipe. In general, the present work aims to prove that by combining the phase and amplitude measurements it is possible to account for electric and dielectric changes in pipelines arising from the flow of water, hydrocarbon and sand.

III. METHODOLOGY

The methodology adopted to assess the feasibility of multiphase flow measurement from electromagnetic signals comprises the following stages:

– Solution of the full electromagnetic forward problem to evaluate the effect of combined permittivity and conductivity on the induced signals.

– Assessment of the effect of excitation frequency on the conduction and displacement currents induced in the medium.

– Characterisation of hydrocarbon mixture in pipelines through complex conductivity measurement.

– Pilot experimental study to demonstrate the effect of permittivity and conductivity on both the amplitude and phase angle of the induced voltages arising from a number of phantom setups.

The following subsections detail the methods employed to address the first three stages above via numerical modelling as well as the experimental technique undertaken for the pilot study.

A. NUMERICAL MODELING

The approach used to solve the electromagnetic problem numerically is based on the solution of the governing Maxwell's equations using the finite element method. In the present study, the commercial software package COMSOL Multiphysics® was used to solve the electromagnetic problem. The numerical simulations consider vacuum conditions and insulated environments that disregard the electromagnetic noise and the interference of external sources. Model validation was carried out by evaluating the performance of the model under conditions with readily known responses.

Typical non-metallic pipelines for multiphase transport in the oil and gas industry range from 2 inch to 8 inch diameter. Accordingly, for the 3D numerical model an averaged pipe size equivalent to a nominal 4 SCH STD was used. The 3D model accounts for a dual coil system built using a current driven coil domain with an initial current phase angle at 0 deg at the transmitter coil and open-circuit approach for the receiving coil. The sensors were located opposite to each other across the pipe cross-section.

Three scenarios were modelled for which the conductivity and permittivity of the medium were swept over the values summarised in **TABLE 1**. The listed values of the dielectric constants reflect a range of fluids readily available in multiphase flow transport, e.g. air ($\varepsilon_r = 1$), natural gas ($\varepsilon_r = 1.2$), octane ($\varepsilon_r = 2$), oil ($\varepsilon_r = 2.8$), water ($\varepsilon_r = 80$), and dry limestone ($\varepsilon_r = 7$) [25]–[27]. The 99 conductivity-permittivity combinations accounted for various ratios of water, hydrocarbon and sand content. The volume fraction of the fluids in the pipe were also varied by changing the size of the cylindrical inclusion to account for segregated annular flow configurations.

The quasi-static premise states that if the permittivity of a material at a given frequency is very small compared to its

TABLE 1. Conductivities and relative permittivities used in simulations.

Property / Fluid	Gas	Oil	Sand	Water
Conductivity (S/m)	0	0	0	0.5, 0.15, 0.25, 0.35, 0.45, 0.55, 1, 5
Dielectric Constant ($\varepsilon/\varepsilon_0$)	1	2, 2.8, 3, 3.2, 4	5, 6.03, 7.4, 10	80

conductivity ($\sigma \gg \omega\varepsilon_0\varepsilon_r$) the displacement currents can be ignored. In this study a broad range of $\sigma/\omega\varepsilon_0\varepsilon_r$ relationships are assessed, ranging from 1.121E-1 to 8.99E4 for excitation frequencies between 1Mz and 100MHz. Our hypothesis is that for $\sigma/\omega\varepsilon_0\varepsilon_r$ ratios below 1E3 the displacement currents have a significant effect in the electromagnetic measurements, through which non-conductive flow characterisation can be achieved.

B. EXPERIMENTAL STUDY

A high-speed MIT system was used to conduct experiments aiming to validate the simulation and discuss the system requirements necessary to monitor hydrocarbon and sand transportation. The high data acquisition speed (500 fps) of the system used is key to allow characterisation of transient structures without missing any relevant physical phenomena. The meter comprised 8 induction sensors. The sensors were equally spaced around the perimeter of a vertically arranged pipe section of 600 mm long, with an internal diameter of 100 mm, in agreement with the geometry simulated. All the inductive sensors were alternately excited yielding a full set of 28 unique inter-sensor measurements. The MIT system used, was originally designed to measure the phase shift of the induced sine wave. The amplitudes of the induced voltages were not designed as a system default output, because of the need to prioritise and reserve the PFGA communication bandwidth for outputting phase angles at 500 Hz. However, the amplitudes of the voltage can be post-processed using stored digitised analogue signals from each channel within the FPGA memory buffer.

The pilot tests comprise measurement of the phase angle and the voltage amplitude via semi-static and static tests, i.e.:

– Semi-static test aimed at assessing the dynamic range of the phase measurements resulting from changing concentrations in water-sand flow. The experiment accounts for 3534 cm^3 of saline water as the continuous phase within the pipe at the beginning of the test. Then 1000 cm^3 of sand was injected at the top of the vertical pipe section, previously filled with saline water, in a steady continuous motion yielding a stream of sand flow.

– Static amplitude measurements of the induced voltages were taken from a pipe full (uniform distribution) of air ($\varepsilon_r = 1$), velocite oil ($\varepsilon_r = 2.06$), dry paving sand ($\varepsilon_r = 2.95$), and sand wetted with saline water ($\varepsilon_r = 80$, $\sigma = 3$ S/m). For each condition, ten sets of the digitised analogue signals from the receiving sensors were exported from the FPGA memory. The total test time was 113 s including 10 s period for transferring those exported files to a local memory. The signals from all the receiving sensors given a unique driving channel were captured at the same time. The induced voltage amplitudes were post-processed which constitutes the 'low-speed' amplitude data.

IV. RESULTS AND DISCUSSION

The present section discusses the results of the numerical scenarios evaluated and the experiments undertaken. The discussion is structured in three main sections, the first one evaluates the macroscopic electromagnetic behaviour of various materials usually found in oil transport systems. The identification of the influence of the fluid properties on the electromagnetic measurements builds up to a further application study in section B, where the characterisation of the susceptibility of the system to the intrinsic properties of the hydrocarbons, sand and water is presented. Following, Section C discusses the results from the pilot study that demonstrates the proof-of-concept.

A. MACROSCOPIC ELECTROMAGNETIC BEHAVIOUR OF MATERIALS

This section addresses the effects of frequency excitation and spatial fluid configuration on the intensity of the induced currents. Furthermore, it characterises the electromagnetic behaviour of the meter to various flow mixtures by addressing the influence of permittivity and conductivity on the signal measured by the receiving sensor across a pipeline.

1) INFLUENCE OF PERMITTIVITY AND CONDUCTIVITY ON THE INDUCED CURRENTS

Aiming to evaluate the performance of the system measurements for various excitation frequencies and their impact on the signal received, conduction and displacement current densities were computed for selected scenarios and presented following. The induced currents were calculated within the pipe by integrating the norm of the current density over the fluid volume. The selected scenarios are summarised in **TABLE 2**.

Figure 1 shows the effect of varying the frequency on the displacement and conduction current densities. For frequencies of 20 MHz and lower, the norm of the conduction currents was linearly proportional to the excitation frequency and remained the same for a fixed value of conductivity, irrespective of the permittivity of the medium (see **Figure 1(a)**). Similarly, mainly the permittivity changes are reflected in the displacement current density, with virtually no changes due to variations in conductivity (see **Figure 1(b)**). The displacement currents are proportional to the frequency squared, and remained nearly constant regardless of the conductivity changes, although a slight difference is seen for larger permittivity values as the frequency increases.

TABLE 2. Simulation parameters for evaluation of excitation and displacement currents.

Conductivity (S/m)	[0.55,1,3,5]
Dielectric Constant ($\varepsilon/\varepsilon_0$)	[2,7.4,70, 75, 80]
Operating Frequency (Hz)	[1E6, 5E6, 1E7, 2E7, 1E8]

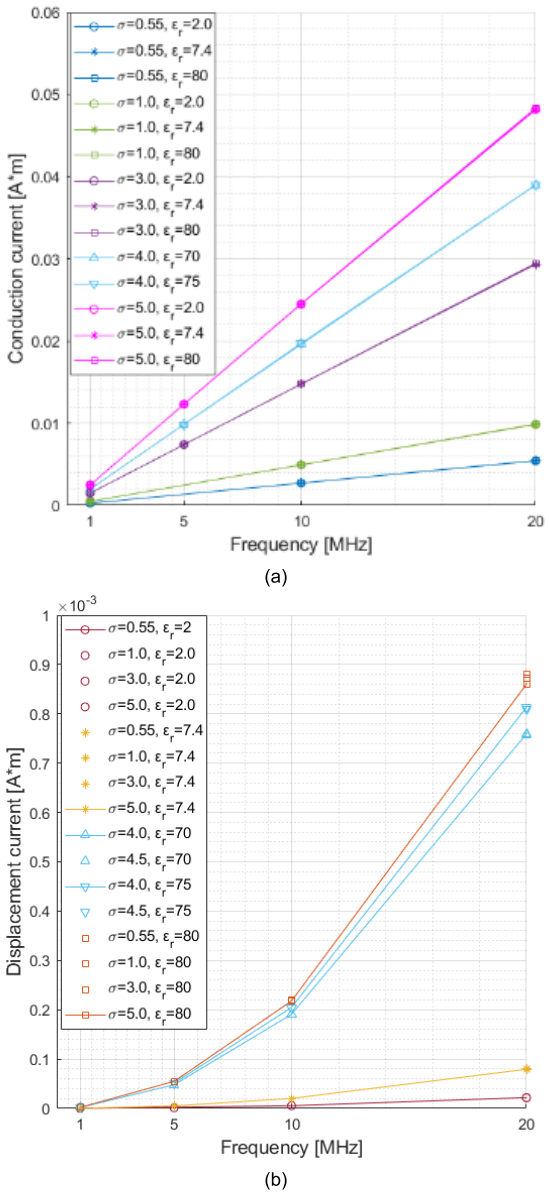

FIGURE 1. Effect of the frequency in (a) conduction currents and (b) displacement currents of phases of various conductivities and permittivities.

For measurement of fluid conductivity in a multiphase flow, excitation frequencies between 1 and 40 MHz are typically used, as within these frequencies the displacement currents are in a similar order with the eddy currents [28].

However, in the present study an extra step was considered in order to investigate the frequency dependence of the induced currents accounted for a higher excitation frequency of 1E8 Hz. At such high frequency, both the permittivity and conductivity have a combined effect on the induction and conduction currents (see **Figure 2**).

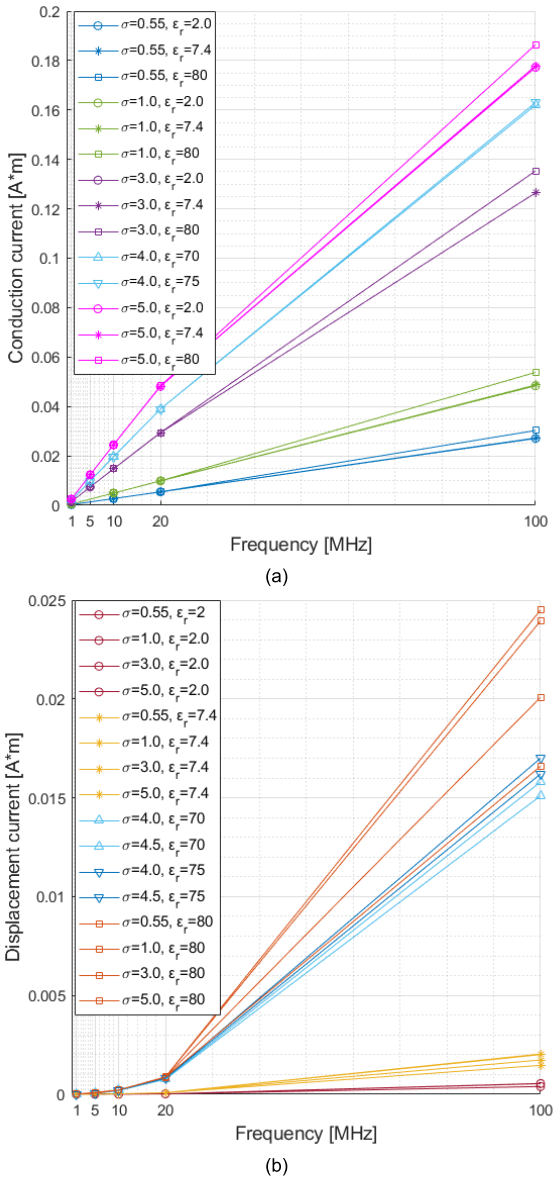

FIGURE 2. Variation of (a) conduction currents and (b) displacement currents of phases of various conductivities and permittivities for excitation frequencies of 1 to 100 MHz.

This outcome is attributed to the change in polarization mechanism, which would preclude any direct correlation between the electric and dielectric properties of the medium and the measurement signals.

2) INFLUENCE ON THE INDUCED CURRENTS OF CHANGES IN THE SPATIAL DOMAIN

Multiphase flow accounts for high complexity of spatial and temporal distributions of the phases. The assessment of the effect of non-uniform distributions on the received signals is based on evaluation of spatial changes of flow mixtures. These spatial changes considered a cylindrical inclusion of various lengths located in the middle of the pipe. The volumetric fractions assessed comprise the following

range $\alpha = [1.0, 0.9, 0.8, 0.7, 0.5, 0.3]$. The changes on displacement and conduction currents at 10MHz for the given volume fractions are presented in **Figure 3**. Results show that displacement and conduction current densities are affected by changes in volume for scenarios of fixed permittivity and conductivity.

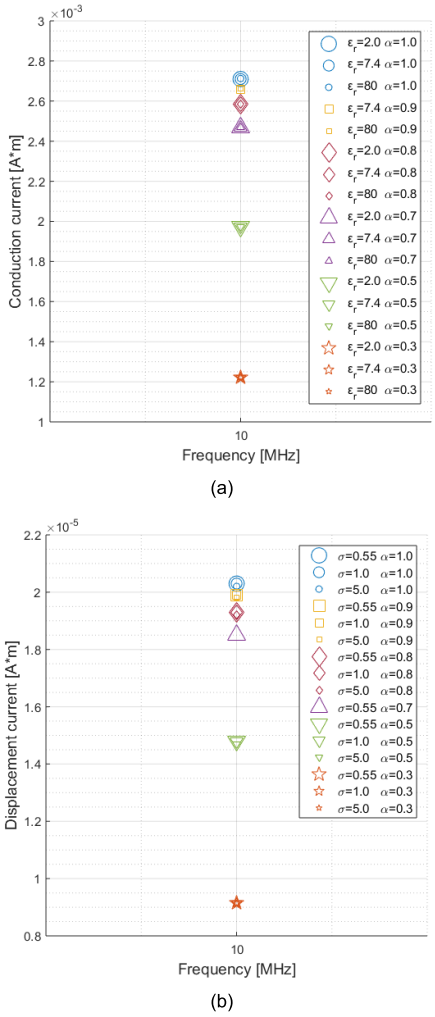

FIGURE 3. Effect of changes in volume fraction with variations in (a) conduction currents for a mixture conductivity of 0.55 S/m and (b) displacements currents for a mixture relative permittivity of 7.4.

Figure 4 contrasts the variation in the current densities due to changes in volume for various conductivities and permittivities. The variation in the induced current densities is relatively linear with volumetric changes. The variation of the induced currents per volumetric fraction change is quadratic as represent by the trends in the inner boxes. The change in the slope of the induced currents shows that, given the model setup, the received signals are highly sensitive to changes of volume fractions in the vicinity of the sensor array.

3) INFLUENCE OF PERMITTIVITY AND CONDUCTIVITY ON THE INDUCED ELECTROMAGNETIC SIGNAL

Here an analysis of the system response to changes in the electrical and dielectric properties of the fluids is presented.

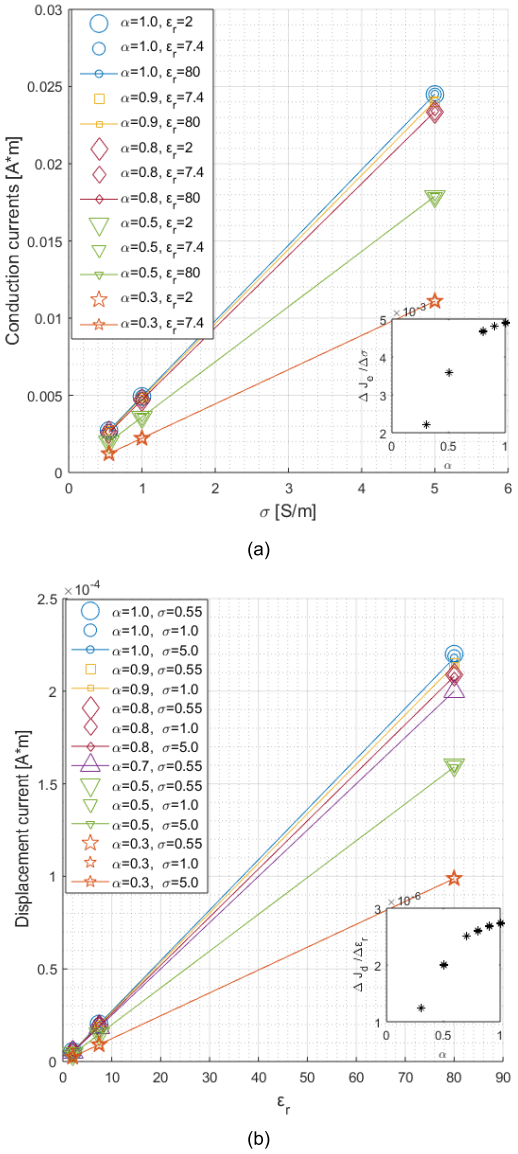

FIGURE 4. Effect of changes in volume fraction on (a) induced conduction and (b) displacement currents.

The influence of the fluid conductivity on the induced absolute amplitude and the phase angle of the signal measured at the opposite receiving coil are shown in **Figure 5(a)** and **(b)**, respectively.

It is evident that the conductivity has a significant impact on both measured signals. Particularly, the phase angle shows that shifts arise from induced eddy currents around a conductive phase in a multiphase flow, where the relative permittivity of the flow have negligible effect. The same outcome is evidenced for the real component of the magnitude, as illustrated in **Figure 6**.

Conversely, the dielectric constant is mainly reflected on the imaginary component of the amplitude and on the absolute amplitude signal, **Figure 7(a)** and **(b)**, respectively. These amplitude signals, however, form a complex measurement that encompasses combined information regarding the

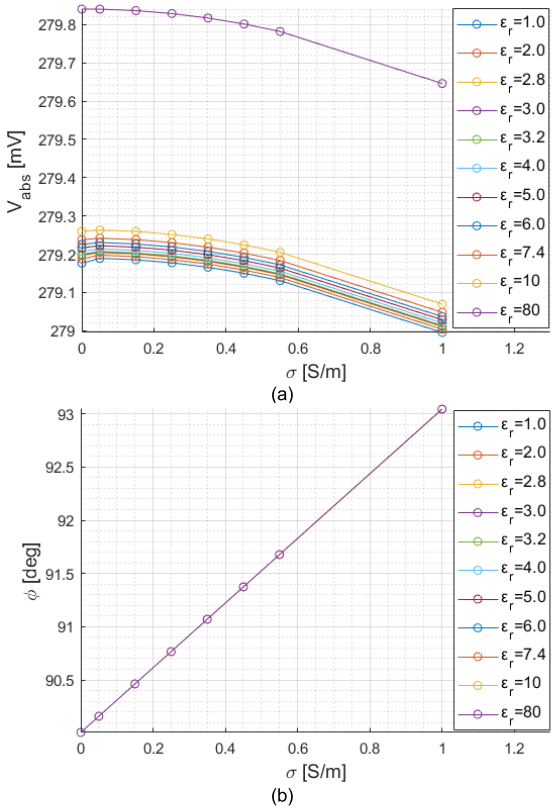

FIGURE 5. Effect of changes in conductivity on the (a) absolute amplitude and (b) phase angle measured at the receiving sensor.

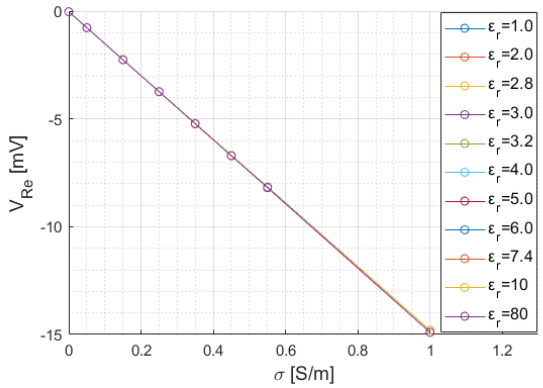

FIGURE 6. Effect of changes in conductivity on the real component of the measured amplitude.

displacement currents induced by the dielectric medium and the conductive currents induced in the conductive phase in a multiphase flow. This complex measurement is reflected in the boxes of the respective **Figure 7(a)** and **(b)**.

Contrasting the absolute amplitude and its imaginary component, results in the former providing a larger dynamic range of the two. The results, however, identify that the effect of permittivity in the overall amplitude signal is at least one order of magnitude greater than that observed on independently measuring the real and imaginary components separately. This outcome is associated to the inverse effect that the conductivity has on both amplitude components, decreasing

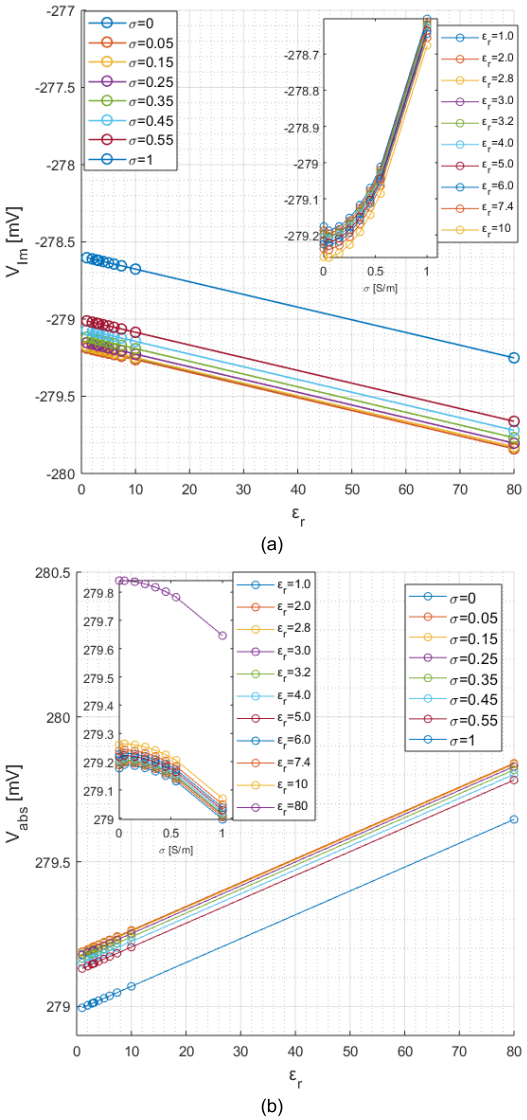

FIGURE 7. Effect of changes in permittivity on (a) the imaginary component of the amplitude and (b) absolute amplitude signal.

the dynamic range of the absolute amplitude signal, and hence increasing the relative impact of the permittivity in the measurement.

B. CHARACTERISATION OF HYDROCARBON MIXTURE IN PIPELINES THROUGH COMPLEX CONDUCTIVITY MEASUREMENT

1) INFLUENCE OF CHANGES IN THE SPATIAL DOMAIN ON THE INDUCED ELECTROMAGNETIC SIGNAL

An evaluation on the effect that non-conductive fluids have on the induced signals is presented here. The simulation approach accounted for mixed flow, e.g, distributed bubble or slurry forming a core bulk with changing mixture permittivity. The fraction of mixture occupying the pipe (α) was varied systematically. **Figure 8(a)** shows that variations in the measured amplitude due to changes in volume fraction of both sand and gas in the non-conductive mixture are linear

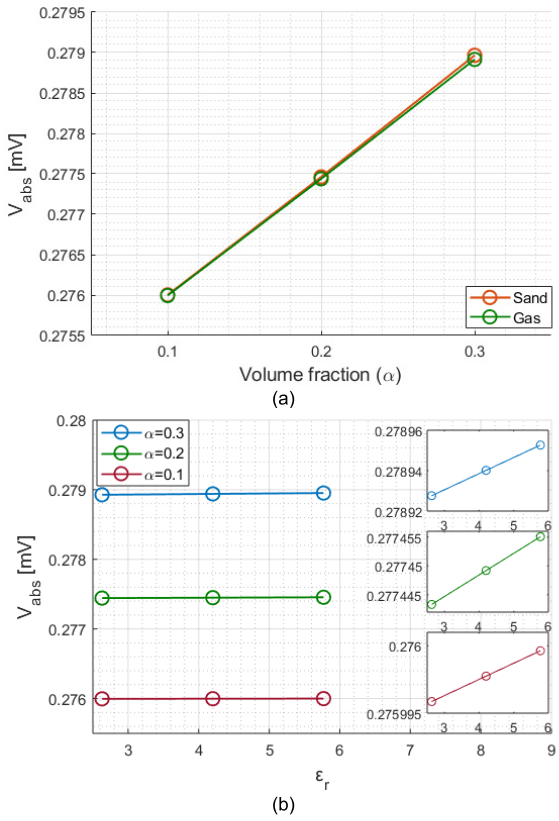

FIGURE 8. Results of induced absolute amplitude from (a) sand ($\varepsilon_r = 7.4$) and gas ($\varepsilon_r = 1$) and (b) various permittivity mixtures.

and in the order of 1.5mV per every 10% increase. The changes in amplitude due to variations in the permittivity of the mixture are also linear but much smaller than those seen for changes in volume fraction **Figure 8(b)**.

The ratio of the variation of amplitude to that of the variation of permittivity is shown in **Figure 9**. The trend is nonlinear and accounts for variations in the microVolts range per every permittivity shift, which constitutes a challenge for data acquisition systems.

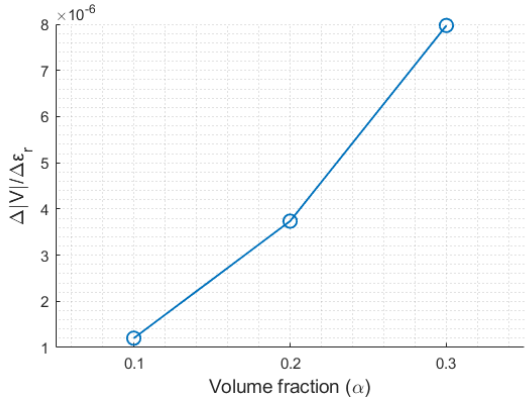

FIGURE 9. Amplitude dynamic range for changes in permittivity and volume.

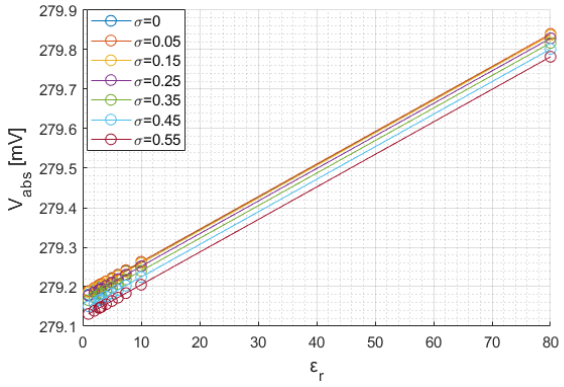

FIGURE 10. Change in amplitude of the induced voltage with relative permittivity changes for a given mixed flow conductivity range (0.05-0.5S/m).

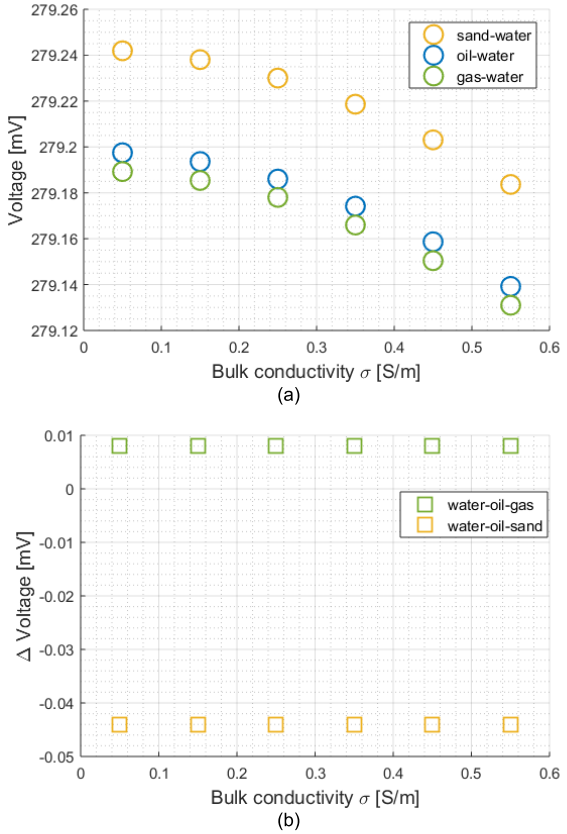

FIGURE 11. Induced voltage from (a) a trio of two-phase flows water-oil ($\varepsilon_r = 2$), water-gas ($\varepsilon_r = 1$), and water sand ($\varepsilon_r = 7.4$) and (b) the signal difference between the water-oil and the water-gas flows (labelled water-oil-gas) and the water-oil and the water-sand flows (labelled water-oil-sand) in low conductive environments ($\sigma = 0.05$-0.5S/m).

2) ELECTROMAGNETIC SIGNALS FOR MULTIPHASE FLOW IN PIPELINES

By using extensive computational models, the weighting of the conductivity and permittivity to the measured signals are assessed to better understand from which electrical properties the voltage measurements are stemming, at any given condition. **Figure 10** shows that for mixed flows with conductivity less than 0.5 S/m, typical for low water contents, the change

in amplitude of induced voltage has a linear relationship with relative permittivity of the mixed flow.

Figure 11(a) shows the received signals from three two-phase systems within low bulk conductive environments. The evaluated mixtures comprise water-oil, water-gas and water-sand flows with relative permittivity of 2, 1, and 7.4, respectively. The difference between the received voltages is constant throughout the bulk conductivity range. This allows contrasting three phase flow scenarios containing both oil and water combined with either gas or sand. **Figure 11(b)** evidences that the change in the signals results solely from the change in the relative permittivity of the gas and the sand. The influence in the receiving signal of the water-oil-sand flow to that of the water-oil-gas flow is given by a 4.4:1 ratio.

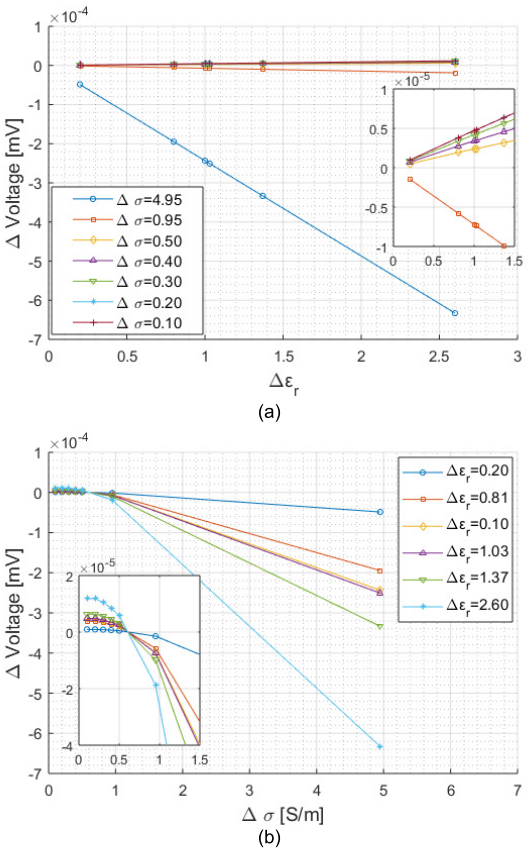

FIGURE 12. Changes in the amplitude of the induced voltage for various mixed relative permittivity and bulk electrical conductivities.

Figure 12 shows the amplitude of the induced voltage for variations in the relative permittivity in various conductive environments. For a given bulk conductivity below 1 S/m, the change in amplitude of the induced voltage increases as relative permittivity of the mixed flow increases (see box in **Figure 12(a)** and **Figure 12 (b)**). In contrast, as the water content increases creating a mixture conductivity of 1 S/m or greater, the change in amplitude of the induced voltages is dominated by the conductivity increase (also evident in **Figure 7(b)**). This behaviour is more pronounced when the conductivity difference of the mixed flow is superior to 4 S/m, similar of that of formation water and slurries.

C. PERMITTIVITY AND CONDUCTIVITY MEASSUREMENT CAPABILITY

1) SEMI-STATIC CONDUCTIVITY MEASUREMENT CAPABILITY

A semi-static test was undertaken aiming to reproduce water and sand two-phase flow. The experiment used saline water (3 S/m) as the initial continuous medium at the start of the experiment. Subsequently, the phase angle was measured as the sand was introduced into the pipeline after 20s of tests (frame 1E4 in **Figure 13**).

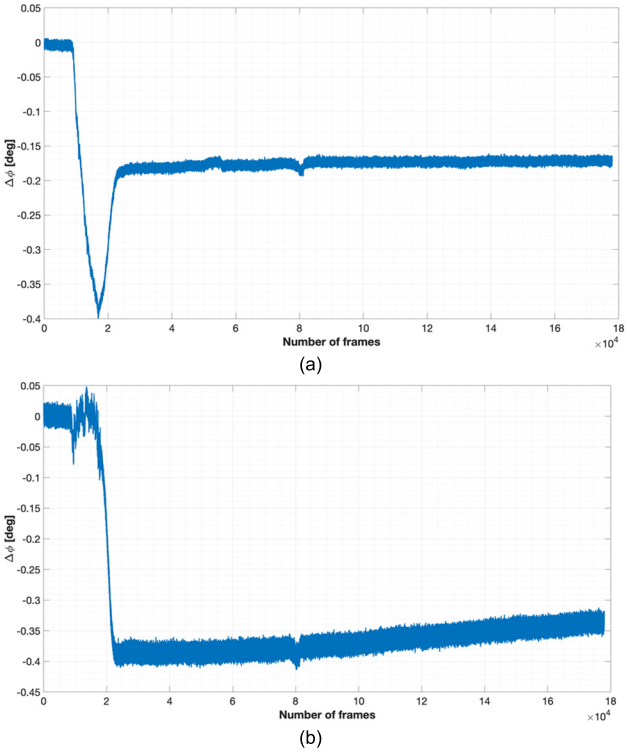

FIGURE 13. MIT phase shifts for sand-in-water flow from (a) neighbouring sensor-pair and (b) opposite sensor-pair.

Figure 13 shows the phase shift measurements from the neighbouring and across-the-pipe (opposite) sensor-pairs as a result of water and sand flow. These sensor-pairs were chosen because their measurements yield the smallest and largest phase shifts, thus encompassing the entire phase dynamic range. The phase dynamic range is defined by the phase shift measured by the neighbouring sensor (*ns*) in the lower end of the spectrum and the opposite sensor (*os*) in the higher end, i.e, $\Delta\theta_{range} = [\Delta\theta@ns, \Delta\theta@os]$. Hence, the selected sensor measurements provide an overview of the measurement capability range of the measurement system. The authors corroborated that the trends are consistent for all sensor-pairs sharing the same relative position to the excitation sensor.

The phase in **Figure 13** shift refers to water as the reference medium. The phase measurements seen after frame 1E4 result from the variation of the volume fraction of water as the sand stream flows into the pipe occupying a fraction of the cross section. Overall, the experimental system measures an approximate phase shift of 0.4 deg as a result of the decrease

in bulk conductivity yielding from the flow of sand across the measurement planes (frames 1E4 to 3E4) and the resulting phase configuration once the sand is settled at the bottom of the pipe section (frames 3E4 and above).

The phase measurements show that the MIT system is sensitive to changes in conductivity and volume fraction, demonstrating once again the robustness of the technology for measurement of conductivity contrasts. Knowledge of the conductivity distribution within the pipe, derived from the phase shift, combined with amplitude measurements provide the opportunity to also differentiate between materials of different permittivities. With this in mind, the following section addresses the capabilities of the MIT system to measure both permittivity and conductivity changes through the induced voltage amplitude.

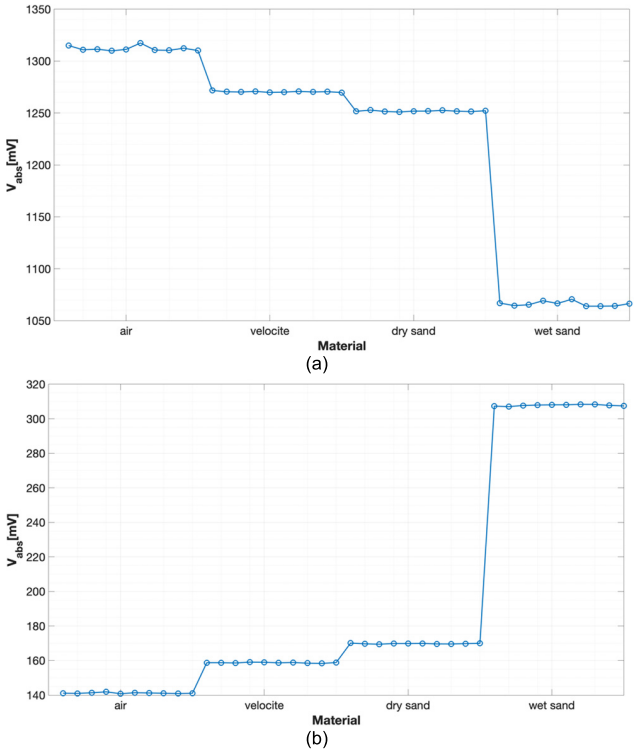

FIGURE 14. Amplitude voltage for various materials measured from (a) neighbouring sensor-pair and (b) opposite sensor pair.

2) COMBINED PERMITTIVITY AND CONDUCTIVITY MEASUREMENTS FROM ELECTROMAGNETIC INDUCED SIGNALS

Figure 14 shows the results of the amplitude measurements yielding from the static tests performed using materials of various permittivies and conductivities, i.e., air, velocite oil, dry sand and wet sand respectively; where air, velocite and dry sand have relative permittivity of 1, 2.06 and 2.95. Their conductivities are negligible. The wet sand was created by mixing the pure saline with a conductivity of 3 S/m into the dry sand until the sand were fully wet visually, representing a medium, with both conductivity and permittivity.

Ten sets of voltage amplitudes for every material are shown in a consecutive order of increasing medium permittivity. Consistently, measurements from neighbouring and opposite sensor-pairs are shown in **Figure 14(a)** and **(b)**, respectively. As before, these sensor-pairs were chosen because their measurements yield the largest and smallest induced voltages as the distances between the excitation and receiving sensors increase, thus encompassing the entire amplitude dynamic range framed by the amplitude measured by the opposite sensor (*os*) in the lower end of the spectrum and the neighbour sensor (*ns*) in the higher end, i.e, $V_{abs\_range} = [V_{abs}@os, V_{abs}@ns]$.

The results show four clearly differentiable levels of amplitudes for different medium. The difference in amplitude among the non-conductive materials, i.e. air, oil and dry sand, indicate that the measured signal is stemming from the induced displacement currents, as discussed in Section B2.

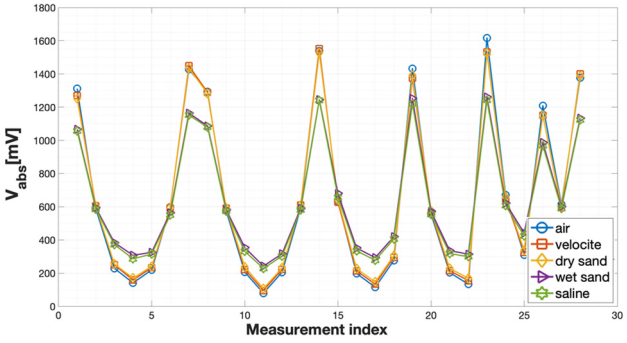

FIGURE 15. MIT full set of voltage measurements for pipe full of air, velocite oil, dry sand, wet sand and saline water.

Figure 15 shows the average of the ten sets voltage measurements for every material and all 28 unique measurement pairs. The dynamic range of the induced voltage is consistent among non-conductive materials; namely, air, velocite oil, and dry sand as well as between the conductive medium, i.e. wet sand and pure saline water; but is different between conductive and non-conductive materials. This variation is in agreement with the simulations results, and responds to the combined effect that both permittivity and conductivity have on the amplitude signal, as evidenced in **Figure 7(b)** and **Figure 12**.

The relationship between the relative permittivity and the induced voltages for neighbouring and opposite sensors is shown in **Figure 16(a)** and **(b)**, respectively. The results combined convey the largest differences in the electromagnetic induced amplitude expected from changes in the permittivity of the medium for pipe-full scenarios. The relationship is within the milliVolts range. However, recalling from Section B1, smaller phase volume fractions result in voltage shifts within the microVolts range.

The amplitude and phase measurements derived from the pilot tests demonstrated the capability of MIT to measure permittivity and conductivity changes This capability could potentially result in three phase measurements through MIT.

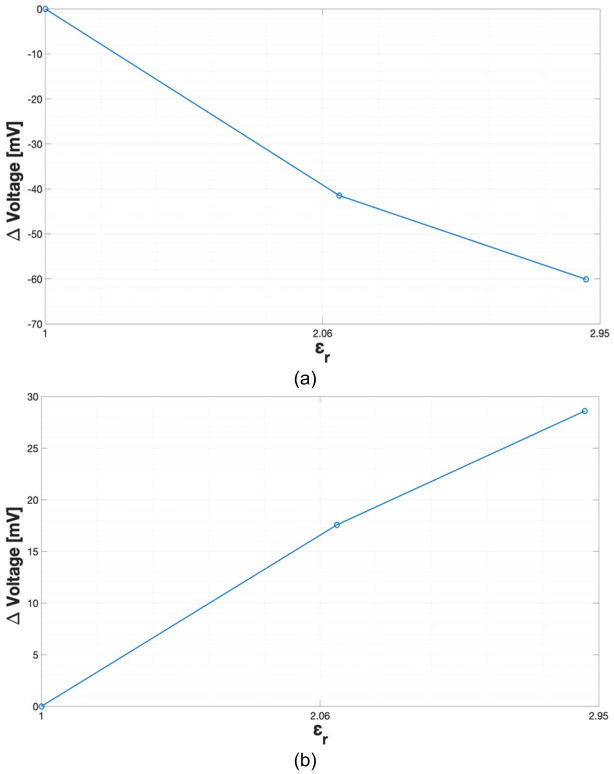

FIGURE 16. Amplitude range voltage for various permittivities in a non-conductive environment from (a) neighbouring sensor-pair and (b) opposite sensor-pair.

V. CONCLUSION

The present study expands on the existing literature and addresses the feasibility of deriving the permittivity from electromagnetic measurements. The range of electric properties that are relevant to the intended application was derived. The degree of correlation between the measurements and the electric properties, as well as a correlation model that comprises the simultaneous responses from the system to changes in permittivity and conductivity, was presented.

This work disclosed that for a given three-phase flow of water-oil-sand or water-oil-gas with low water contents (bulk conductivity ranging from 0.05 to 0.6S/m), the change in amplitude of the induced voltage is influenced by the permittivity of the fluids. Hence, electromagnetic induction can be used to measure both the phase shift and amplitudes of the complex voltages to continuously monitor and measure the phase fraction of conductive and non-conductive phases. Furthermore, it was verified that the effect of permittivity in the absolute amplitude signal is at least 1 order of magnitude greater than that observed on the real and imaginary components disjointedly. These results provide improvements to previous approaches where electromagnetic signals were de-multiplexed for measurement in low conductive environments.

The concept of permittivity measurement through MIT was demonstrated via a pilot test. It was shown that, in order to differentiate between non-conductive materials while also measuring changes in conductivity across the cross-section, the system requires: (i) inclusions of skin depth much larger than the sample dimensions, (ii) high speed system with both voltage amplitude and phase angle output (500 fps was seen to suffice for the semi-static tests conducted here), and capabilities (iii) to measure voltage amplitudes within the microvolts range, and (iv) to measure phase shifts below a fraction of a degree.

The results presented are of particular interest for low conductive mixtures, where the measured signal is predominantly dominated by the permittivity, i.e., the volumetric fractions of the oil, gas and sand. This novel approach yields real-time derivation and verification of the conductive and non-conductive phase volumetric using a single apparatus. Hence, removing the need to co-locate two separate metering systems.

The use of amplitude signals that provide information related to the dielectric properties for non-conductive phase for multiphase fractions allows multiphase measurement over the same cross-section, enhancing the measurement accuracy and broadening the application spectrum of electromagnetic based imaging technologies for in-situ flow pattern imaging.

REFERENCES

[1] G. Falcone and B. Harrison, "Forecast expects continued multiphase flowmeter growth," *Oil Gas J.*, vol. 109, no. 10, pp. 25–34, 2011.
[2] R. Thorn, G. A. Johansen, and B. T. Hjertaker, "Three-phase flow measurement in the petroleum industry," *Meas. Sci. Technol.*, vol. 24, pp. 1–17, 2012, doi: 10.1088/0957-0233/24/1/012003.
[3] FLEXIM. (2019). *Flow Measurement of Slurry*. Accessed: Jul. 21, 2019. [Online]. Available: https://www.flexim.com/en/industry-solutions/mining/flow-measurement-slurry-tailings-paste-fill-70-solids
[4] H. Griffiths, "Magnetic induction tomography," in *Electrical Impedance Tomography. Methods, History and Applications*, D. Holder, Ed. London, U.K.: IOP, 2005.
[5] R. A. Albrechtsen, Z. Z. Yu, and A. J. Peyton, "Preliminary Experiments on the Investigation of the Inductive Technique for Measuring Water Cotent in Muti-Phase Flow," *Proc. ECAPT*, Bergen, Norway, 1995, pp. 2005–2013.
[6] J. Xiang, Y. Dong, M. Zhang, and Y. Li, "Design of a magnetic induction tomography system by gradiometer coils for conductive fluid imaging," *IEEE Access*, vol. 7, pp. 56733–56744, 2019, doi: 10.1109/ACCESS.2019.2914377.
[7] L. Ma, A. Hunt, and M. Soleimani, "Experimental evaluation of conductive flow imaging using magnetic induction tomography," *Int. J. Multiphase Flow*, vol. 72, pp. 198–209, Jun. 2015, doi: 10.1016/j.ijmultiphaseflow.2015.02.013.
[8] L. Ma, D. McCann, and A. Hunt, "Combining magnetic induction tomography and electromagnetic velocity tomography for water continuous multiphase flows," *IEEE Sensors J.*, vol. 17, no. 24, pp. 8271–8281, Dec. 2017.
[9] M. Zolgharni, P. D. Ledger, and H. Griffiths, "Forward modelling of magnetic induction tomography: A sensitivity study for detecting haemorrhagic cerebral stroke," *Med. Biol. Eng. Comput.*, vol. 47, no. 12, pp. 1301–1313, Dec. 2009, doi: 10.1007/s11517-009-0541-1.
[10] S. Watson, R. J. Williams, W. Gough, and H. Griffiths, "A magnetic induction tomography system for samples with conductivities below 10 S/m," *Meas. Sci. Technol.*, vol. 19, no. 1, pp. 1–11, 2008, doi: 10.1088/0957-0233/19/4/045501.
[11] H. Yazdanian and R. Jafari, "Improving the temporal resolution of magnetic induction tomography for molten metal flow visualization," *IEEE Trans. Instrum. Meas.*, vol. 59, no. 1, pp. 553–557, Mar. 2010.
[12] H. Scharfetter, R. Casanas, and J. Rosell, "Biological tissue characterization by magnetic induction spectroscopy (MIS): Requirements and limitations," *IEEE Trans. Biomed. Eng.*, vol. 50, no. 7, pp. 870–880, Jul. 2003, doi: 10.1109/TBME.2003.813533.

[13] R. Casañas, H. Scharfetter, A. Altes, A. Remacha, P. Sarda, J. Sierra, R. Merwa, K. Hollaus, and J. Rosell, "Measurement of liver iron overload by magnetic induction using a planar gradiometer: Preliminary human results," *Physiol. Meas.*, vol. 25, no. 1, pp. 315–323, Feb. 2004, doi: 10.1088/0967-3334/25/1/035.
[14] L. Ma and M. Soleimani, "Magnetic induction spectroscopy for permeability imaging," *Sci. Rep.*, vol. 8, no. 1, Dec. 2018, Art. no. 7025, doi: 10.1038/s41598-018-25507-4.
[15] E. Michel, D. Hernandez, and S. Y. Lee, "Electrical conductivity and permittivity maps of brain tissues derived from water content based on T1-weighted acquisition," *Magn. Reson. Med.*, vol. 77, no. 3, pp. 1094–1103, Mar. 2017, doi: 10.1002/mrm.26193.
[16] H. Griffiths, W. Gough, S. Watson, and R. J. Williams, "Residual capacitive coupling and the measurement of permittivity in magnetic induction tomography," *Physiol. Meas.*, vol. 28, no. 7, pp. S301–S311, Jul. 2007, doi: 10.1088/0967-3334/28/7/S23.
[17] M. Zhang, L. Ma, and M. Soleimani, "Dual modality ECT–MIT multiphase flow imaging," *Flow Meas. Instrum.*, vol. 46, pp. 240–254, Dec. 2015, doi: 10.1016/j.flowmeasinst.2015.03.005.
[18] H. Scharfetter, R. Merwa, and K. Pilz, "A new type of gradiometer for the receiving circuit of magnetic induction tomography (MIT)," *Physiol. Meas.*, vol. 26, no. 2, pp. S307–S318, Apr. 2005.
[19] H. Ammari, A. Buffa, and J.-C. Nedelec, "A justification of eddy current model for the maxwell equations," *SIAM J. Appl. Math.*, vol. 60, no. 5, pp. 1805–1823, 2000.
[20] K. Schmidt, O. Sterz, and R. Hiptmair, "Estimating the eddy-current modeling error," *IEEE Trans. Magn.*, vol. 44, no. 6, pp. 686–689, Jun. 2008, doi: 10.1109/TMAG.2008.915834.
[21] B. Lambert, *Dielectric Spectroscopy*. Hattiesburg, MN, USA: The Univ. of Southern Mississippi, 2018. Accessed: Nov. 14, 2018. [Online]. Available: https://web.archive.org/web20060118002845/http://psrc.usm.edu/mauritz/dilect.html
[22] R. Dorey, *Ceramic thick firlms for MEMS and Microdeviced*. Amsterdam, The Netherlands: Elsevier, 2012.
[23] M. Wang, *Industrial Tomography: Systems and Applications*. Amsterdam, The Netherlands: Elsevier, 2015.
[24] M. Soleimani, "Computational aspects of low frequency electrical and electromagnetic tomography: A review study," *Int. J. Numer. Anal. Model.*, vol. 5, no. 3, pp. 407–440, 2008.
[25] E. F. May, T. J. Edwards, A. G. Mann, and D. K. Manning, "Density, dielectric constant and PVT measurements of a gas condensate fluid," *J. Petroleum Sci. Eng.*, vol. 41, no. 4, pp. 297–308, Feb. 2004, doi: 10.1016/j.petrol.2003.10.001.
[26] E. ToolBox. (2008). *Dielectric Constants of common Liquids*. Accessed: Jul. 30, 2019. [Online]. Available: https://www.engineeringtoolbox.com/liquid-dielectric-constants-d_1263.html
[27] W. P. Clement. (1999). *Dielectric Constants for Earth Materials*. Accessed: Jul. 30, 2019. [Online]. Available: http://www.geo.umass.edu/faculty/wclement/dielec.html
[28] W. Yin, A. J. Peyton, G. Zysko, and C. Ktistis, "Evaluation of the radiative wave propagation effect in EMT," *Int. J Inf. Syst. Sci. Spec. Issue Comput. Asp. Soft F. Tomogr.*, vol. 2, no. 4, pp. 575–584, 2006.

YESSICA ARELLANO received the B.E. and M.Sc. degrees from the La Universidad del Zulia, in 2005 and 2011, respectively, the M.Sc. degree (Hons.) from Robert Gordon University, in 2008, and the Ph.D. degree (research) in fluid and complex systems from Coventry University, targeted tomography measurements of multiphase flow. For a period of 11 years, she was a member in offshore fields with the Facilities Department, Oil and Gas Industry, Venezuela. She was a Research and Development Engineer in fluid mechanics with INTEVEP S.A.

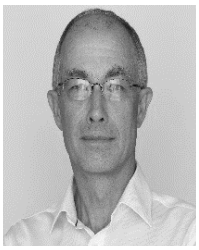

ANDY HUNT received the B.Sc. degree in aeronautical engineering from the University of Bristol, U.K., in 1978, and the Ph.D. degree in aerodynamics from Cranfield University, U.K., in 1982. He was a Postdoctoral Research Fellow and a Lecturer with the University of Surrey. He spent a period of 15 years with the Oil Industry, Schlumberger, one of the world's Big Three Oilfield Service companies, where he was the Head of the Fluid Dynamics Research and the Product Development Director. He has been a Visiting Professor with The University of Manchester, from 1996 to 2002. He was also the Vice-President of the Institute of Measurement and Control, from 2002 to 2007. He is currently a Technical Director with iPhase Ltd., and the CEO of Atout Process Ltd, U.K. He is also a Chartered Engineer with the Fellow of the Institute of Measurement and Control.

LU MA received the Ph.D. degree in electronic and electrical engineering from the University of Bath, in 2014. She was a Postdoctoral Researcher with the Engineering Tomography Laboratory. She is currently a Chartered Engineer with the Institute of Measurement and Control and a Principal Engineer with iPhase Ltd., where she leads the development of a non-radioactive and non-invasive in-situ real time multiphase flow meter for the energy sector. She also sits on the Ph.D. Supervisory Panel with the Centre for Flow Measurement and Fluid Mechanics, Coventry University. Her research interests include electrical imaging techniques, multiphase flow measurement, electromagnetic sensors and instrumentation, and non-destructive evaluation.